PCCP

Accepted Manuscript

ROYAL SOCIETY OF CHEMISTRY

www.rsc.org/pccp

PCCP

PAPER

Electronic Structures of Anatase $(TiO_2)_{1-x}(TaON)_x$ Solid Solutions: First-Principles Study †

Received 11th April 2015, Accepted

DOI: 10.1039/x0xx00000x

www.rsc.org/pccp

Wenqiang Dang,[a] Hungru Chen,[b] Naoto Umezawa,[b] and Junying Zhang*[a]*

Sensitizing wide band gap photo-functional materials under visible-light irradiation is an important task for efficient solar energy conversion. Although nitrogen doping into anatase TiO_2 has been extensively studied for this purpose, it is hard to increase nitrogen content in anatase TiO_2 because of the aliovalent nitrogen substituted for oxygen, leading to the formation of secondary phases or defects that hampers the migration of photoexcited charge carriers. In this paper, electronic structures of $(TiO_2)_{1-x}(TaON)_x$ ($0 \le x \le 1$) solid solutions, in which the stoichiometry is satisfied with the co-substitution of Ti for Ta along with O for N, are investigated within the anatase crystal structure using first-principles calculations. Our computational results show that the solid solutions have substantially narrower band gaps than TiO_2, without introducing any localized energy states in the forbidden gap. In addition, in comparison with the pristine TiO_2, the solid solution has a direct band gap when the content of TaON exceeds 0.25, which is advantageous for light absorption. The valence band maximum (VBM) of the solid solutions, which is mainly composed of N 2p states hybridized with O 2p, Ti 3d or Ta 5d orbitals, is higher in energy than that of pristine anatase TiO_2 consisting of non-bonding O 2p states. On the other hand, incorporating TaON into TiO_2 causes the formation of d-d bonding states through π interactions and substantially lowers the conduction band minimum (CBM) because of the shortened distance between some metal atoms. As a result, the anatase $(TiO_2)_{1-x}(TaON)_x$ is expected to become a promising visible-light absorber. In addition, some atomic configurations are found to possess exceptionally narrow band gaps.

1. Introduction

Since the discovery of Fujishima and Honda effect in 1972,[1] photocatalysis has drawn extensive attention both in the fields of environmental remediation and energy conversion. Titanium dioxide (TiO_2), the most well-known photocatalyst, is active only under ultraviolet (UV) irradiation, and exhibits poor performance under the shine of visible light which accounts for the majority of sunlight. One effective way to enhance the visible-light photocatalytic activity is doping nonmetal ions (such as C, N, B, S and F),[2-9] metal ions[10,11] or both[12-15] into the TiO_2 lattice to introduce extra energy states in the band gap. In general, the doping concentration especially that of the cations is less than 10 at%, because the dopants usually has limited solubility in the TiO_2 matrix and high dopant concentration deduces the formation of secondary compound. Replacing oxygen by nitrogen in TiO_2 could substantially shift the photo-absorption edge, leading to the visible-light photocatalytic activity.[2,7-9,16] However, it was reported that when N concentration exceeds over the solubility limit, nitrogen atoms start to occupy interstitial sites, leading to transformation from the active anatase to less-active rutile phase.[17] Heavily N-doped anatase TiO_2 up to 15% was grown by a novel epitaxial method,[18] although it is still challenging to achieve such a high concentration of nitrogen in a powder formed sample for photocatalysis application. As a result, the band structure was unable to be tuned in a large scale. In addition, in such doped TiO_2 photocatalysts, it's the dopants that cause visible-light absorption, thus the absorption coefficient depends on the concentration of dopants. As a consequence, only a small modification of the photoabsorption edge can be expected by the doping scheme. Furthermore, the impurity levels created by dopants in the forbidden band of the material are usually discrete, which would appear disadvantageous for the migration of photogenerated holes. In contrast, solid solution contains N as constituent element that forms the top of the valence band. Thus, photogenerated holes can migrate smoothly in the valence band of the material, which is particularly advantageous for water oxidation involving 4-electron transfer.[19] Up to now, the maximum solubility has been obtained in the TiO_2-ZrO_2 system,[20,21] incorporating up to 30 at% ZrO_2 into TiO_2, which enhanced the photocatalytic activity under UV light irradiation but failed under visible light because ZrO_2 has larger band gap than TiO_2.

High visible light photocatalytic activity has been realized in other systems than TiO_2 by forming solid solution using two materials with a similar crystal structure. For example, a new type of oxynitride with a unique composition and structure was obtained by compositing GaN and ZnO, both possessing wide

[a] Department of Physics, Beihang University, Beijing 100191, China. E-mail: zjy@buaa.edu.cn; Tel: +86-10-82315351; Fax: +86-10-8231-7931
[b] Environmental Remediation Materials Unit, National Institute for Materials Science, Ibaraki 305-0044, Japan. E-mail: umezawa.naoto@nims.go.jp; Tel: +81-29-860-4547; Fax: +81-29-860-4958
† Electronic Supplementary Information (ESI) available: See
DOI: 10.1039/x0xx00000x

band gap with a wurtzite-type structure, which achieved water splitting into H_2 and O_2 under visible light irradiation.[22,23] A novel series of perovskite-type solid solution photocatalysts $AgNbO_3$-$SrTiO_3$ were powerful for oxidizing H_2O into O_2 from aqueous $AgNO_3$ solution under visible light. [24] Solid solution β-$AgAl_{0.6}Ga_{0.4}O$ exhibited 35 and 63 times higher photocatalytic activities than two terminus materials β-$AgAlO_2$ and β-$AgGaO_2$. [25] Solid solution $(AgIn)_xZn_{2(1-x)}S_2$ is an active photocatalyst for H_2 evolution under visible-light irradiation even though $AgInS_2$ and ZnS hardly possesses any activity under visible-light irradiation.[26]

δ-TaON phase (anatase-type structure) tantalum oxide nitride powder was successfully prepared by reaction of gaseous ammonia with an amorphous tantalum oxide precursor. [27] Anatase TaON film with band gap of 2.37 eV was obtained by using nitrogen plasma assisted pulsed laser deposition.[28] J. Grins et al. prepared $(TiO_2)_{1-x}(TaON)_x(0.52<x<0.87)$ solid solution with anatase structure by ammonolysis of Ti-Ta gels.[29] These reports suggest that $(TiO_2)_{1-x}(TaON)_x$ has a potential to be used as a visible-light photocatalytic solid solution. Herein, we studied the crystal and electronic structures of $(TiO_2)_{1-x}(TaON)_x$ solid solutions (x=0.25, 0.5, 0.75) using first-principles calculations. The band gaps of the solid-solution narrow in comparison with that of TiO_2, but is not a simple function of x. Increasing TaON content tunes the solid solution from indirect band gap to direct band gap, without forming any localized energy bands. This is different with the N and Ta co-doped TiO_2 by R. Long et al. [14] They found that incorporation of Ta and N into TiO_2 leads to the formation of continuum-like fully occupied N 2p-Ta 5d hybridized states above the top of the valence band as well as Ta 5d orbitals located at the bottom of the conduction band. As for anatase TaON whose photocatalytic activity has not been evaluated experimentally, we theoretically determined the CBM and VBM positions, demonstrating its great potential as a visible-light responsive photocatalyst, in agreement with the previous study of T. Lüdtke et al., indicating that δ-TaON is a promising photocatalytic material for water splitting.[27]

2. Calculation methods

The density functional theory (DFT) calculations were performed using the spin-polarized projector augmented wave (PAW) pseudopotentials[30] via the Vienna Ab initio Simulation Program (VASP). [31] The exchange and correlation energy was treated using the generalized gradient approximation (GGA) via Perdew-Burke-Ernzerhof (PBE) prescription. [32] The constituted atomic valence states adopted were N $2s^22p^3$, O $2s^22p^4$, Ti $3p^63d^34s^1$ and Ta $5p^66s^15d^4$. The plane wave cut-off energy was 500 eV and a $13\times13\times5$ grid of Monkhorst-pack points were employed for geometry optimization of a 12-atom conventional cell of anatase TiO_2. Geometry optimization was performed until the total energy difference reached 10^{-5} eV and the residual forces on atoms were less than 0.01 eV/Å. During the geometry optimization, volume and shape of the cell as well as atomic positions were relaxed.

To construct model structures for the anatase solid solution $(TiO_2)_{1-x}(TaON)_x$, we incorporated Ta and N atoms into lattice sites of a 12-atom anatase TiO_2, taking x value of 0.25, 0.5 and 0.75. Here, we considered all the possible lattice sites (see Fig. S1 and table S1, ESI) that Ta and N could occupy i.e., 4, 19 and 28 configurations for x=0.25, 0.5 and 0.75, respectively, and found the model structure that yields the lowest total energy through geometry optimizations for the volume and shape of the cell as well as atomic positions. For anatase TaON, we studied the most plausible six atomic configurations within the 12-atom cell. The geometry relaxations were performed in the same way as the solid solutions. The most stable configuration have $I4_1md$ symmetry, in agreement with the previous studies. [27, 29,33, 34]

3. Results and discussion

3.1 Optimized crystal structure

Fig. 1(a) shows the optimized anatase TiO_2. The lattice constants are a=3.81Å, b=3.81 Å, c=9.69 Å, very similar with experimental results.[35] Figures 1(b)-1(e) show the most stable configurations of the anatase $(TiO_2)_{1-x}(TaON)_x$ solid solutions at different concentrations, i.e., x= 0.25, 0.5, 0.75 and 1.0. Fig. 1(f) is the variation of the cell volume of the most stable $(TiO_2)_{1-x}(TaON)_x$ versus x value, indicating approximately linear cell increase when content of TaON increases in the solid solution because of the larger lattice constants of TaON than TiO_2, agreeing well with the experimental results.[29]

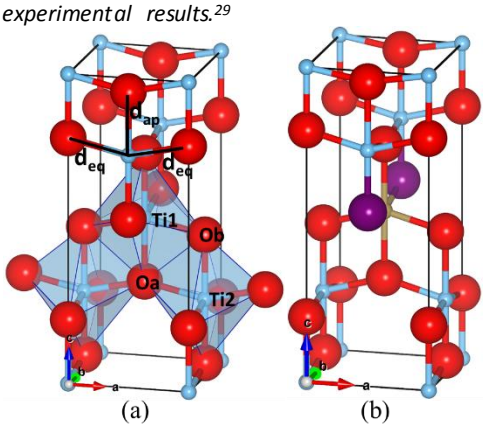

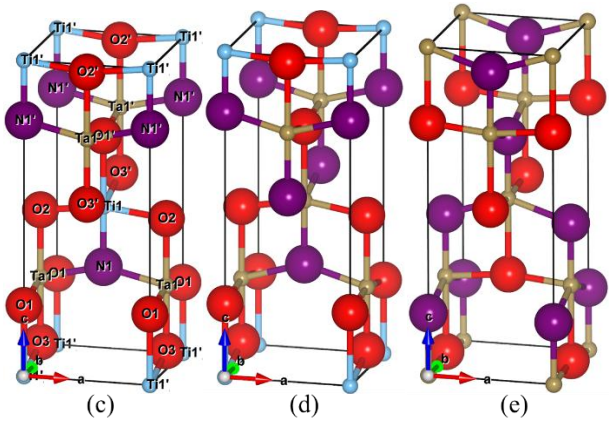

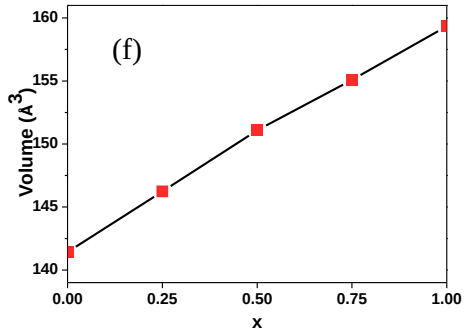

Fig. 1 *Optimized crystal structure of $(TiO_2)_{1-x}(TaON)_x$ when x=0 (a), 0.25(b), 0.5 (c), 0.75 (d), 1.0 (e), variation of the cell volume (f) versus TaON content . Red, purple, blue and brown balls represent oxygen, nitrogen, titanium and tantalum ions, respectively. The definition of the apical (d_{ap}) and equatorial (d_{eq}) bond lengths is indicated.*

In the solid solution, metal T (T=Ti or Ta) coordinates with O or N to form octahedron. The cation-anion bond lengths are different along the apical (d_{ap}) and equatorial (d_{eq}) directions defined in Fig. 1. All the cation-anion bond lengths in the solid solution are listed in table 1.

The enthalpy of mixing E_x for a cell with 12 atoms was obtained from the formula,

$$E_x = E_s - (1-x)E_{TiO_2} - xE_{TaON} \quad (1)$$

where E_s, E_{TiO2}, and E_{TaON} are the calculated total energies of $(TiO_2)_{1-x}(TaON)_x$, TiO_2, and TaON, respectively, which are obtained from our DFT calculations for the 12-atoms anatase models. The enthalpies of mixing of the solid solution are slightly positive ($E_{0.25}$=0.19eV, $E_{0.5}$=0.09eV and $E_{0.75}$=0.18 eV), indicating that the formation of solid solutions $(TiO_2)_{1-x}(TaON)_x$ is endothermic. Experimentally, this drawback can be overcome by precisely controlling epitaxial methods or soft chemical methods that are not bound by thermodynamic stability.

Table 1 *Cation-anion bond lengths in different directions in the solid solution*

x	Ti-O (Å)	Ti-N (Å)	Ta-O (Å)	Ta-N (Å)
0	1.95 (d_{eq})			
	2.01 (d_{ap})			
0.25	1.93~1.99 (d_{eq})		1.97 (d_{eq})	2.00 (d_{eq})
	1.96~2.13 (d_{ap})	1.93 (d_{ap})	2.08~2.09 (d_{ap})	
0.5	1.96~2.01 (d_{eq})		1.97 (d_{eq})	2.02 (d_{eq})
	2.22 (d_{ap})	1.88 (d_{ap})	2.04~2.09 (d_{ap})	
0.75	1.97 (d_{eq})		1.97~1.99 (d_{eq})	1.98~2.04 (d_{eq})
		1.86 (d_{ap})	2.22~2.30 (d_{ap})	1.98~2.01 (d_{ap})
1			2.01 (d_{eq})	2.01 (d_{eq})
			2.15 (d_{ap})	2.17 (d_{ap})

3.2 Band alignment

In this section, we discuss the band alignment of the solid solutions $(TiO_2)_{1-x}(TaON)_x$ in comparison with their limiting phases TiO_2 and TaON. To estimate a band edge position of $(TiO_2)_{1-x}(TaON)_x$ with respect to that of TiO_2, we have performed a DFT calculation for an interface $(TiO_2)_{1-x}(TaON)_x/TiO_2$ following the method proposed by Janotti et al. [36 - 39] The interface model was built by stacking three unit cells of $(TiO_2)_{1-x}(TaON)_x$ on top of three unit cells of TiO_2 along the c direction forming 72-atom supercell. Since the lattice constants of TiO_2 (p for short) and $(TiO_2)_{1-x}(TaON)_x$ (s for short) are different, we took average in-plane lattice constants, i.e. $a=(a_p+a_s)/2$ and $b=(b_p+b_s)/2$, for the construction of the interface models. Geometry relaxations were performed only for c axis with the averaged in-plane lattice constants fixed to take into account the Poisson ratio. The averaged electrostatic potentials over atoms (V_{ref} $[...]_{interface}$) for $(TiO_2)_{1-x}(TaON)_x$ and TiO_2 in the interface model are estimated from the mid layer of each material which is far distant from the interface and can represent bulk region. We then define the difference of the averaged electrostatic potentials of the two materials as

$$\Delta V_{ref} = V_{ref}\,[(TiO_2)_{1-x}(TaON)_x]_{interface} - V_{ref}\,[TiO_2]_{interface}.$$

Coming back to the bulk, the highest-occupied states ε_{VBM} [...], averaged electrostatic potentials (V_{ref} $[...]_{bulk}$), and band gaps E_g[...] for $(TiO_2)_{1-x}(TaON)_x$ and TiO_2 are also estimated from our DFT calculations using the 12-atom cell. Finally, the valence band and conduction band offsets of $(TiO_2)_{1-x}(TaON)_x$ with respect to TiO_2 are obtained from

$$\Delta\varepsilon_{VBM} = (\varepsilon_{VBM}[(TiO_2)_{1-x}(TaON)_x] - V_{ref}\,[(TiO_2)_{1-x}(TaON)_x]_{bulk}) - (\varepsilon_{VBM}[TiO_2] - V_{ref}\,[TiO_2]_{bulk}) + \Delta V_{ref},$$

$$\Delta\varepsilon_{CBM} = \Delta\varepsilon_{VBM} + E_g\,[(TiO_2)_{1-x}(TaON)_x] - E_g\,[TiO_2].$$

The obtained band alignment is shown in Fig. 2. It is understood that the VBM and CBM of $(TiO_2)_{1-x}(TaON)_x$ (x=0.25, 0.5, and 0.75) respectively shift upwards and downwards with respect to those of TiO_2, leading to band gap narrowing. In the case of a pristine anatase TaON, the CBM is much more negative than that of TiO_2, indicating a promising material for highly active photocatalytic water reduction.

The obtained band alignment is shown in Fig. 2. It is understood that the VBM and CBM of $(TiO_2)_{1-x}(TaON)_x$ (x=0.25, 0.5, and 0.75) respectively shift upwards and downwards with respect to those of TiO_2, leading to band gap narrowing. In the case of a pristine anatase TaON, the CBM is much more negative than that of TiO_2, indicating a promising material for highly active photocatalytic water reduction.

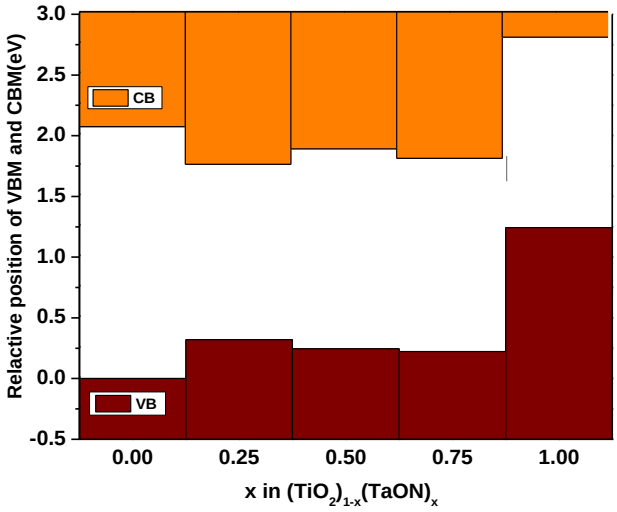

Fig. 2 *The schematic band edges. The zero energy is at the valence band maximum of pristine TiO_2.*

3.3 Electronic structures

The relative band edge positions are rationalized by detailed analysis of electronic structures of the solid solutions. The density of states (DOS) for $(TiO_2)_{1-x}(TaON)_x$ are presented in Fig. 3 and Fig. S2 (ESI), where the energy is referenced to the VBM of a pristine TiO_2 and the band offsets discussed in the previous paragraph are taken into account for $(TiO_2)_{1-x}(TaON)_x$. In pristine TiO_2, the VBM and CBM mainly consist of O 2p and Ti 3d states, respectively. After one fourth of TiO_2 is substituted by TaON, the CBM is still dominated by Ti 3d orbitals, while a hybrid band of N 2p, O 2p, Ti 3d and Ta 5d is observed at the VBM. When the content of TaON increases to half in the solid solution, the DOS is very similar with that of $(TiO_2)_{0.75}(TaON)_{0.25}$, except some Ta 5d orbitals appear at the CBM. The hybridization of N 2p, O 2p and cation d orbitals is pronounced near the VBM. With increasing TaON content in the solid solution, Ta 5d orbitals contribute further to the VBM and CBM character as shown in Fig. 3 and Fig. S2 (ESI).

The nature of chemical bonds among orbitals that is responsible for the band edges can be visualized by partial electron density (square of the wave function) associated with the energy states at the VBM and CBM as shown in Fig. 4. In TiO_2, the VBM is composed mainly of O 2p non-bonding states, while the CBM is dominated by the Ti 3d non-bonding states as shown in Fig. 4(a), agreeing well with the results reported by Asahi and Y. Taga.[40] In $(TiO_2)_{0.75}(TaON)_{0.25}$, π bonding among Ti 3d states appears in Fig. 4(b), which is substantially different from the non-bonding states of Ti 3d in TiO_2 (Fig. 4(a)). Whereas, hybridization among N 2p, O 2p and Ti d_{xz}-states is observed at the VBM of $(TiO_2)_{0.75}(TaON)_{0.25}$. Similar band characters are found in the other concentrations (x=0.5 and 0.75) as shown in Fig. 4(c) and 4(d). Cation-anion or cation-cation π bond formation is promoted as increase in the TaON content. The electron clouds at the CBM are connected forming a zigzag-like character along d-d π bonds that distribute all over the crystal, while those at the VBM are connected in a xy plane.

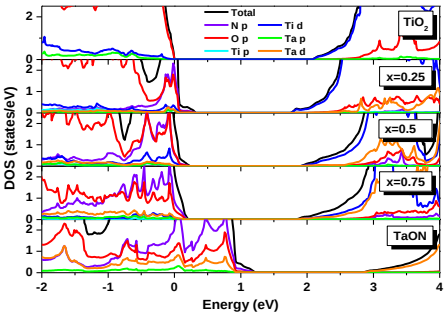

Fig. 3 *Total density of states (TDOS) and partial density of states (PDOS) of $(TiO_2)_{1-x}(TaON)_x$ when x=0, 0.25 , 0.5, 0.75 and 1.0 near the VBM and CBM. The zero energy is at the valence band maximum of pristine TiO_2.*

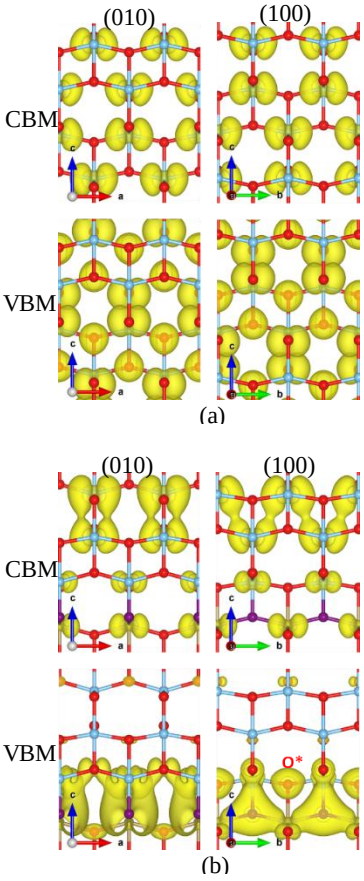

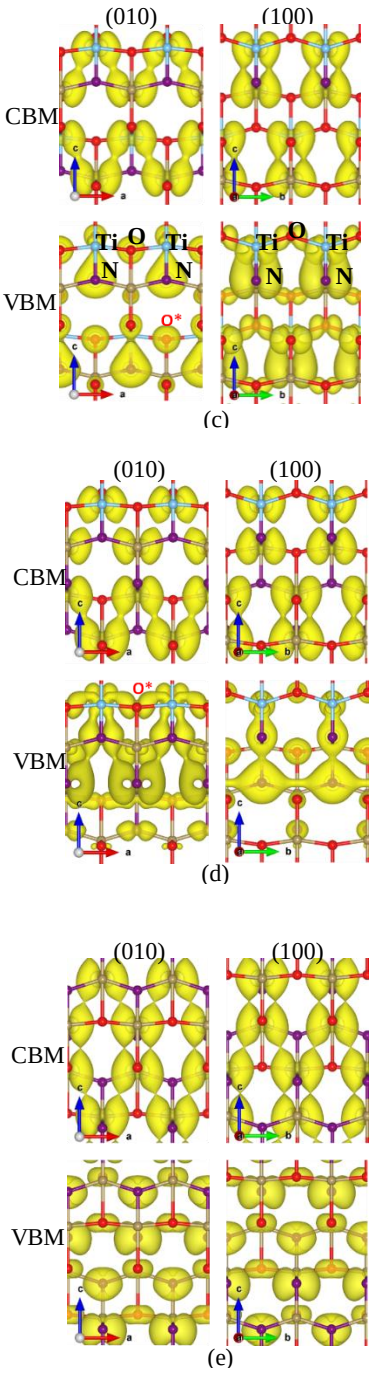

Fig. 4 *The partial electron density at VBM and CBM when x=0 (a), 0.25(b), 0.5(c), 0.75(d), 1.0 (e) at a 0.01 electrons/Å³ isosurface level. The left and right panel indicates the (010) and (100) plane, respectively.*

According to Jeremy K. Burdett et al.,[35] TiO_6 octahedron distortion originated from some inter-constraint factors, such as Coulomb repulsion between neighboring Ti atoms, repulsion between two oxygen atoms on the edges shared by two octahedron (Fig. 1(a)) and attraction between Ti and O. Since ionic radii of four-coordinated N^{3-} is larger than four-coordinated O^{2-} (1.46Å vs. 1.38Å), it is anticipated that three-coordinated N^{3-} is larger than three-coordinated O^{2-}. Meanwhile, six-coordinated Ta^{5+} is larger than six-coordinated Ti^{4+} (0.64Å vs. 0.605Å).[41] As a result, the cell volume increases with increasing the TaON ratio in the solid solution. Furthermore, the Coulomb repulsion between N and O exceeds that between two O atoms, causing the longer N-O distance (2.53Å) than O-O distance (2.48 Å). This repulsion causes the octahedron containing this O atom (denoted as O in Figures 4(b)-4(d)) to have a lower distortion along a Ti-O*-Ti network, namely, its angle closer to 180 degree than in TiO_2. With increasing the TaON ratio in the solid solution, the distortion continues to decrease. The elongation of anion-anion distance in a quadrangle containing two cations and two anions, also causes the cations approach to each other along the z direction, resulting in the attraction of d_{xy} orbitals forming the zigzag-like d-d π bonding network. The π bonding significantly lowers the CBM in the solid solutions compared to the case in TiO_2 in which the CBM consists of non-bonding Ti d states. The rise of the VBM in the solid solutions mainly originates from the fact that the atomic eigenvalues of 2p states are higher in nitrogen than in oxygen. This is still the case in our solid solutions even after the hybridization with d orbitals from Ti or/and Ta. The extended 2p states around N in the solid solutions promote the formation of π bonding with cation d states, which somewhat stabilizes the system shifting the VBM downwards, although the resulted VBM is still higher than that in a pristine TiO_2. As a result of the combined two effects of the rise of VBM and decline of CBM, the solid solutions have narrower band gaps than that of TiO_2.*

In Fig. 5(a)-5(e), band structures along the symmetry directions for the Tetragonal Lattice Brillouin zone (Fig. S3, ESI) for TiO_2, $(TiO_2)_{1-x}(TaON)_x$ (x=0.25, 0.5, and 0.75), and TaON are shown. The pristine TiO_2 has an indirect band gap of about 2.06eV for a transition from M to Γ as exhibited in Fig. 5(a), much smaller than an experimental value 3.2eV,[42] due to the well-known shortcoming of GGA.[43] As mentioned earlier, in $(TiO_2)_{0.75}(TaON)_{0.25}$, the VBM and CBM shift upwards and downwards, respectively, leading to a narrower band gap (1.43eV) compared to the pristine TiO_2 (Fig. 4(b)), while the indirect nature is barely remained for a transition from Z to Γ.

Further increase in the TaON content in the solid solution turns the band transition into direct at Γ. This indicates that the solid solution with a higher TaON content is more suitable for light absorption. Notably, the incorporation of TaON into TiO_2 lattice does not induce any localized energy levels in a forbidden band, unlike low-concentration N-doped TiO_2. R. Long et al. studied the (N, Ta)-codoped TiO_2 via DFT.[14] Their results indicate that codoping N and Ta can effectively enhance N concentration and besides, lead to the formation of continuum-like fully occupied N 2p-Ta 5d hybridized states above the top of the valence band as well as Ta 5d orbitals located at the bottom of the conduction band. However, such an impurity state often produces a small quantity of occupation, resulting in the declined photocatalytic activity under UV irritation although it benefits the activity under visible light.[44,45] The localized energy levels in the forbidden band usually tend to be a recombination center between photogenerated carriers, and the absorption coefficient depends on the concentration of dopants. In contrast, in $(TiO_2)_{1-x}(TaON)_x$ solid solutions, it is N 2p and O 2p orbitals

that form the tops of the valence band, rather than localized states. As a result, forming solid solution not only shifts the photo-absorption edge, but also improve absorption coefficient. The calculated absorption coefficient spectra confirmed this conclusion as shown in Fig. S4 (ESI). The effective masses of VBM holes and CBM electrons were calculated as shown in table S2 (ESI). The effective mass of electrons shows no obvious difference in the solid solution and the pristine TiO_2 until x reaches 0.50, then electrons become much lighter with further increasing TaON content in the solid solution. Notably, the effective mass of holes along two directions in the solid solutions was substantially reduced in comparison with in TiO_2.

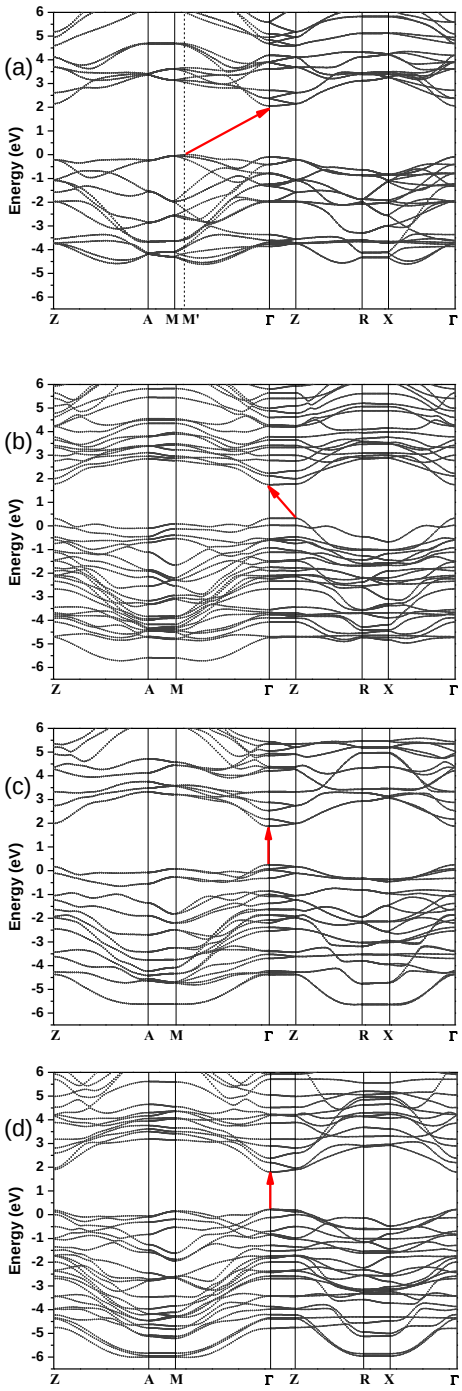

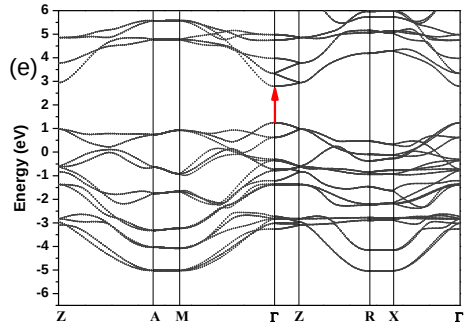

Fig. 5 *Band structure of $(TiO_2)_{1-x}(TaON)_x$ when x=0 (a), 0.25(b), 0.5 (c), 0.75 (d), and 1.0 (e), plotted along the symmetry directions for the Tetragonal Lattice Brillouin zone (Fig. S3, ESI). Red arrow indicates the VBM and CBM. The zero energy is at the valence band maximum of pristine TiO_2.*

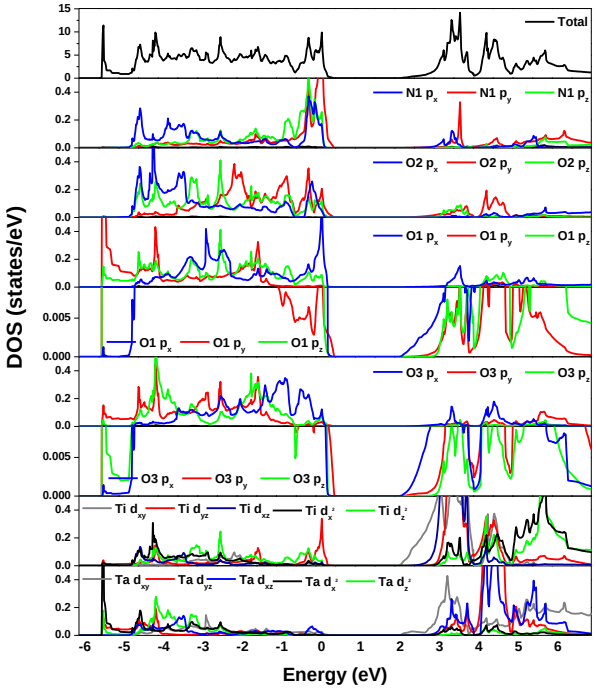

Fig. 6 *PDOS of $(TiO_2)_{0.5}(TaON)_{0.5}$.*

To more thoroughly understand the molecular orbitals of the solid solution, we analyze the PDOS, taking $(TiO_2)_{0.5}(TaON)_{0.5}$ as an example. As can be seen from the crystal structure shown in Fig. 1(c), O1 and O1' occupy the identical sites. So do O2 and O2', O3 and O3', two nitrogen atoms, two titanium atoms and two tantalum atoms. Hence, we choose either one to analyze the PDOS. O2 and N1 atoms form an edge shared by two octahedrons and reside in a same quadrangle, having a similar profile of PDOS, i.e. the highest occupied state consists of anion p_y states as shown in Fig. 6. In anatase structure, an anion is coordinated with three cations in a planner configuration, which is the characteristic of O p-Ti d hybrid states, to form σ bonds and either p_x, p_y, or p_z state, which is orientally perpendicular to the plane, forms a π bond with cation d states. In the case of O2 and N1, p_y state is hybridized with Ti d_{yz} through π interactions. The N1 p_y-Ti d_{yz} π bonds are clearly observed in the partial electron density (Fig. 4(c)). This is the reason for the appearance of p_y at the VBM and its resonance with Ti d_{yz} in PDOS.

The intensity of DOS at the VBM is slightly higher in N1 than in O2 because N 2p states are energetically higher than O 2p states. Similarly, O1 and O3 reside at a quadrangle in yz plane having p_x states dominated near the top of the valence band through the hybridization with Ti d_{xz}, although a small amplitude of p_y appears right at the top of the valence band following the upward shift of Ti d_{yz} that forms σ bonds with p_y. The difference between O1 and O3 in the DOS profile originates from cation coordination, i.e. O1 coordinates with two Ta atoms, while O3 coordinates with two Ti atoms. Ta 5d states are energetically higher than Ti 3d states and their interactions with oxygen p states are limited. In O1, therefore, O p states are intact against hybridization with Ta d states remaining at the VBM, whereas in O3, the hybridization between O p and Ti d is significant, broadening the oxygen band. In fact, a strong σ bond of O3 p_y with Ti d_{yz} is observed in Fig. 4(c). At the CBM, Ti d_{xy} and Ta d_{xy} are also resonant due to their π bonding as discussed earlier, which results in the formation of the lower energy states compared to non-bonding Ti d_{xy} states in a pristine TiO_2.

3.4 Some configurations possessing very narrow band gap

In the above two sections, we presented the crystal structure and electronic structure of most stable configurations in the $(TiO_2)_{1-x}(TaON)_x$ solid solutions. In addition, we found that some models exhibited very small band gap.

For $(TiO_2)_{0.5}(TaON)_{0.5}$, if the atoms are arranged as Fig. 7(a), the band gap is only 0.4 eV as shown in Fig. 7(e). DOS and the partial electron densities of the VBM and CBM in Fig. 7 indicate that the CBM is mainly composed of Ti 3d orbits while the VBM majorly consists of N 2p orbitals, substantially different from the cases shown in Fig. S2(c) (ESI) and Fig. 4(c) in which O 2p orbits contribute approximately half to the VBM besides minor contribution from d states of titanium or tantalum. For $(TiO_2)_{0.5}(TaON)_{0.5}$ with total 19 models, some models have even smaller band gaps (table S1(b), ESI). Similarly with the case in Fig. 7, the VBM majorly consists of N 2p orbits, and CBM is composed by T d_{xy} orbitals. Several models of $(TiO_2)_{0.25}(TaON)_{0.75}$, also possess small band gaps (table S1(c), ESI), have the similar characteristic of the DOS.

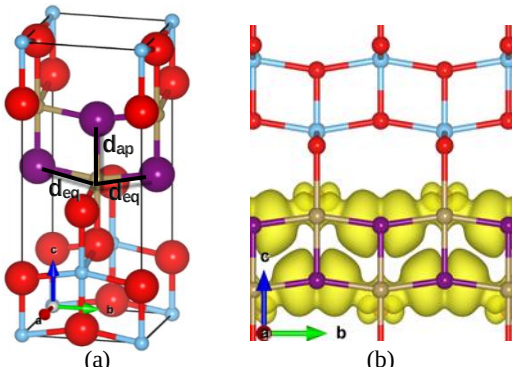

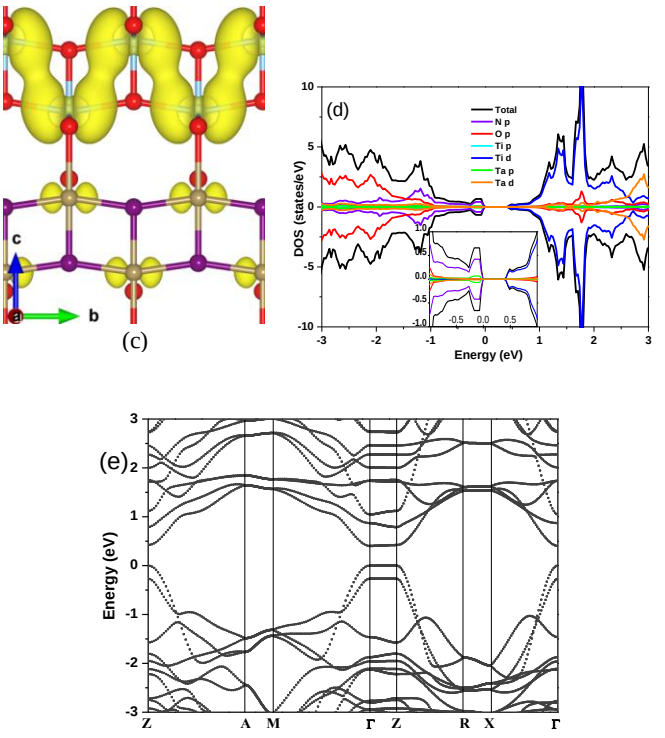

Fig. 7 *One model of $(TiO_2)_{0.5}(TaON)_{0.5}$ that has a small band gap: the crystal structure (a), partial electron density in the VBM (b) and CBM (c) at a 0.01 electrons/Å^3 isosurface level, DOS (d) and band structure (e). The energy band edge in this section was not assigned using the above interface model because we majorly concerned band gap value.*

After thoroughly analyzing the configurations that have much smaller band gaps than the others, we found one common features for these configurations: two N atoms form edge shared by two octahedrons. This is different from the most stable configuration shown in Fig. 1, where N and O form edge shared by two octahedrons. As mentioned above, N has broader electron cloud distribution than O, causing larger Coulomb repulsion. The balance between the repulsions from N-N and the nearby cations leads to the declined distortion in these two octahedrons along the equatorial direction, and hence the N-T-N-T quadrangle approaches to rectangle. As a result, N 2p and Ta 6p form σ bond along the equatorial direction, as shown in Fig. 7(b) and Fig. 8. Because energy level of Ta 6p is higher than that of Ta 5d, the Ta 6p - N 2p bonding states form a σ band above the π band originating from Ta 5d - N 2p bonds, which substantially raises the VBM. On the other hand, similar with the configuration in Fig. 4, the CBM is composed by d-d bonding states with a lower energy than the non-bonding states. These two aspects contribute together to the small band gap of the solid solution (Fig. 7(e)).

We calculated the band gaps and the total energy difference of all the configurations in comparison with the most stable ones as shown in table S1 (ESI). The most stable configurations have the lowest total energy and the largest band gap. The structures, which possess exceptionally narrow band gap, have the highest energy in most cases. This small band gap impedes achieving high photocatalytic activity, but fortunately, they

have high enthalpy of mixing indicating that they have little chance to appear during the experiments. Maybe, these configurations can be obtained, for the special purpose, by employing advanced experimental methods such as the soft chemical synthesis.

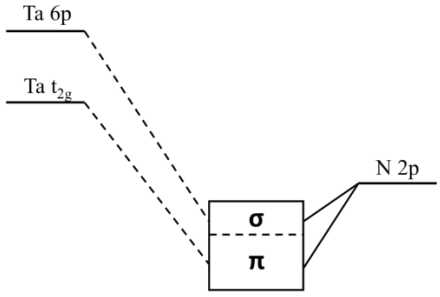

Fig.8 *Schematic molecular orbitals near the VBM in the configurations where two N atoms form an edge shared by two octahedrons.*

4. Conclusions

TaON and anatase TiO_2 can form stable solid solution, while the cell volume increases approximatedly linearly and the inter-band transitions turn from in-direct to direct transitions with increasing TaON content in the solid solution. Introducing TaON into TiO_2 causes the shortened distance between some cations and leads to d-d metallic bonding states instead of non-bonding states, lowering the CBM. Hybridization of N 2p, O 2p and d orbitals from Ti or/and Ta upraises the VMB without forming any localized energy band in the forbidden band. The solid solutions possess higher charge-carrier mobility than the prestine TiO_2 because of the reduced hole effective mass. Anatase TaON has much negative CBM, indicating its potential as a visible-light phtocatalyst to reduce water.

We have found some peculiar configurations with small band gap, in which two N atoms form an edge shared by two octahedrons. The higher Coulomb repulsion of N-N in comparison with O-O and O-N almost deletes the distortion in the T-N_3 (T=Ti or Ta) plane, causing high-energy σ bond of N p-T p at VBM.

In summary, we propose to obtain visible-light anatase photocatalyst by forming solid solution of TaON and TiO_2, realizing high-concentration doping and avoiding the localized energy state.

Acknowledgements

We would like to thank Y. Aoki and J. Ye for useful discussion. This work was supported by Ph. D Programs Foundation of the Ministry of Education of China (Grant No. 20121102110027), and the National Science Foundation of China (Grant Nos. 91222110 and 51472013).

Notes and references

1 *A. Fujishima and K. Honda, Nature 1972,* **238**, *37.*

2 *R. Asahi, T. Morikawa, T. Ohwaki, K. Aoki and Y. Taga, Science 2001,* **293**, *269.*

3 *S. U. M. Khan, M. Al-Shahry, and W. B. I. Jr, Science 2002,* **297**, *2243.*

4 *T. Umebayashi, T. Yamaki, H. Itoh, and K. Asai, Appl. Phys. Lett. 2002,* **81** *(3), 454.*

5 *J. C. Yu, J. G. Yu, W. K. Ho, Z. T. Jiang and L. Z. Zhang, Chem. Mater. 2002,* ***14****, 3808.*

6 *S. In, A. Orlov, R. Berg, F. García, S. Pedrosa-Jimenez, M. S. Tikhov, D. S. Wright and R. M. Lambert, J. Am. Chem. Soc. 2007,* ***129****, 13790.*

7 *C. D. Valentin, G. Pacchioni and A. Selloni, Phys. Rev. B 2004,* **70**, *085116.*

8 *Z. S. Lin, A. Orlov, R. M. Lambert and M. C. Payne, J. Phys. Chem. B 2005,* **109**, *20948.*

9 *J. B. Varley, A. Janotti and C. G. Van de Walle, Adv. Mater. 2011,* **23**, *2343.*

10 *W. Choi, A. Termin and M. R. Hoffmann, J. Phys. Chem. 1994,* ***98****, 13669.*

11 *J. Choi, H. Park and M. R. Hoffmann, J. Phys. Chem. C 2010,* **14**, *783.*

12 *M. E. Kurtoglu, T. Longenbach, K. Sohlberg and Y. Gogotsi, J. Phys. Chem. C 2011,* **115** *(35), 17392.*

13 *M. Y. Xing, Y. M. Wu and J. L. Zhang, Chen F., Nanoscale 2010,* **2**, *1233.*

14 *R. Long and N. J. English, Chem. Phys. Lett., 2009,* **478**, *175.*

15 *T. M. Breault and B. M. Bartlett, J. Phys. Chem. C 2012,* **116**, *5986.*

16 S. Sato, Chem. Phys. Lett. 1986, **123**, 126.

17 T. Okato, T. Sakano and M. Obara, Phys. Rev. B 2005, **72**, 115124.

18 T. L. Chen, Y. Hirose, T. Hitosugi and T. Hasegawa, J. Phys. D: Appl. Phys. 2008, **41**, 062005.

19 K. Maeda, and K. Domen, J. Phys. Chem. C 2007, **111** (22), 7851.

20 B. F. Gao, T. M. Lim, D. P. Subagio and T. Lim, Applied Catalysis A: General 2010, **375**, 107.

21 R. Schiller, C. K. Weiss and K. Landfester, Nanotechnology 2010, **21**, 405603.

22 K. Maeda, T. Takata, M. Hara, N. Saito, Y. Inoue, H. Kobayashi and K. Domen, J. Am. Chem. Soc. 2005, **127**, 8286.

23 K. Maeda, K. Teramura, D. L. Lu, T. Takata, N. Saito, K. Inoue and K. Domen, Nature 2006, **440**, 295.

24 D. F. Wang, T. Kako and J. H. Ye, J. Am. Chem. Soc. 2008, **130**, 2724.

25 S. X. Ouyang and J.H. Ye, J. Am. Chem. Soc. 2011, **133**, 7757.

26 I. Tsuji, H. Kato, H. Kobayashi and A. Kudo, J. Am. Chem. Soc. 2004, **126**, 13406.

27 T. Lüdtke, A. Schmidt, C. Göbel, A.Fischer, N. Becker, C. Reimann, T. Bredow, R. Dronskowski, and M. Lerch, Inorg. Chem., 2014, **53**, 11691.

28 A. Suzuki, Y Hirose., D. Oka, S. Nakao, T. Fukumura, S. Ishii, K. Sasa, H. Matsuzaki and T. Hasegawa, Chem. Mater. 2014, **26**, 976.

29 J. Grins, J. Europ. Ceram. Soc. 1997, **17**, 1819.

30 G. Kresse and D. Joubert, Phys. Rev. B 1999, **59**, 1758.

31 G. Kresse and J. Furthmüller, Phys. Rev. B 1996, **54**, 11169.

32 J. P. Perdew, K. Burke and M. Ernzerhof, Phys. Rev. Lett. 1996, **77**, 3865.

33 T. Bredow, M. W. Lumey, R. Dronskowski, H. Schilling, J. Pickardt, and M. Z. Lerch, Anorg. Allg. Chem. 2006, **632**, 1157.

34 H. Wolff, M. Lerch, H. Schilling, C. Bähtz and R. Dronskowski, J. Sol. Stat. Chem., 2008, **181**, 2684.

35 J. K. Burdett, T. Hughbanks, G. J. Miller, J. W. Richardson, Jr. and J. V. Smith, J. Am. Chem. Soc., 1987, **109**, 3639.

36 C. G. Van de Walle and R. M. Martin, J. Vac. Sci. Technol. B 1987, **5**, 1225.

37 C. G. Van de Walle and R. M. Martin, Phys. Rev. Lett. 1989 **62**, 2028.

38 A. Janotti and C. G. Van de Walle, Phys. Rev. B 2007, **75**, 121201.

39 N. Umezawa, A. Janotti, P. Rinke, T. Chikyow and C. G. Van de Walle, Appl. Phys. Lett., 2008, **92**, 041104.

40 R. Asahi and Y. Taga, Phys. Rev. B 2000, **61**, 7459.

41 R. D. Shannon. Crystal Physics, Diffraction, Acta Crystallogr., Sect. A 1976, **32**, 751.

42 H Tang., H. Berger, P. E. Schmid, F. Levy and G. Burri, Solid State Commun., 1993, **87**, 847.

43 R. O. Jones and O. Gunnarsson, Rev. Mod. Phys. 1989, **61**, 689.

44 J. Wang, D. N. Tafen, J. P. Lewis, Z. L. Hong, A. Manivannan, M. J. Zhi, M. Li and N. Q. Wu, J. Am. Chem. Soc. 2009, **131**, 12290.

45 D. N. Tafen, J. Wang, N. Q. Wu and J. P. Lewis, Appl. Phys. Lett. 2009, **94**, 093101.